Influence of microinclusion in life of rolling elements: Experimental, microstructural, analytical and numerical investigation

Elsevier Editorial System(tm) for
International Journal of Fatigue
Manuscript Draft

Manuscript Number: IJFATIGUE-D-19-00752

Title: Influence of microinclusion in life of rolling elements: experimental, microstructural, analytical and numerical investigation and on balls

Article Type: Original Research Paper

Keywords: Bearing; Microinclusion; Life estimation; ball spin; ball precession.

Corresponding Author: Mrs. raffaella sesana, Ph.D

Corresponding Author's Institution: politecnico di torino

First Author: raffaella sesana, Ph.D

Order of Authors: raffaella sesana, Ph.D; Enrico Ossola; Stefano Pagliassotto; Sebastiano Rizzo; Eugenio Brusa, Full Professor

Manuscript Region of Origin: Europe

Abstract: Rolling contact fatigue is the main cause of failure in bearings. Among other factors, damage phenomena are related to material properties, manufacturing processes and damage evolution might be affected by microinclusions in the material, related to composition, dimension, shape and position of microinclusions. The investigated material is 100Cr6. Relation between microin-clusions and fatigue life is investigated for both specimens undergoing rotating bending fatigue and balls undergoing Hertzian pressure fatigue. A life model for balls, involving microinclusions effect and actual ball rotation movements within the bearing is proposed. Failures are analysed to relate life of roll-ing elements to the microinclusion parameters.

Research Data Related to this Submission

There are no linked research data sets for this submission. The following reason is given:
Data are already presented in the paper

Cover Letter

POLITECNICO
DI TORINO
Dipartimento
di Ingegneria Meccanica
e Aerospaziale

Corso Duca degli Abruzzi, 24
10129 Torino - Italy
Telefono ++39.011.5646905
Telex 220646 POLITO I
Telefax ++39.011.5646999

Torino August 10th 2019

To Editor: José António Correia

International Journal of Fatigue

Object: Paper submission for Special Issue "Metal Fatigue"

Apologizing for the delay, please find attached the first revision to the manuscript
"Influence of microinclusion in life of rolling elements: experimental, microstructural, analytical and numerical investigation and on balls"
We will be pleased to answer any question or communications.
Thanks in advance

Best regards

Raffaella SESANA

Influence of microinclusion in life of rolling elements: experimental, microstructural, analytical and numerical investigation and on balls

R. Sesana[a*], E. Ossola[a], S. Pagliassotto[b], S. Rizzo[b], E.Brusa[a]

[a]*DIMEAS, Politecnico di Torino, Italy*

[2] *Central Lab - Product Development, Tsubaki Nakashima, Italy*

*raffaella.sesana@polito.it

Abstract. Rolling contact fatigue is the main cause of failure in bearings. Among other factors, damage phenomena are related to material properties and manufacturing processes and the damage evolution might be affected by microinclusions present in the material. This influence is related to composition, dimension, shape and position of microinclusions. The investigated material is 100Cr6. Relation between microinclusions and fatigue life is investigated for both specimens undergoing rotating bending fatigue and balls undergoing Hertzian pressure fatigue. A life model for balls, involving microinclusions effect and actual ball rotation movements within the bearing is proposed. Failures are analysed to relate life of rolling elements to the microinclusion parameters.

Keywords: Bearing; Microinclusion; Life estimation; ball spin; ball precession.

1 Introduction

Different damage phenomena can affect bearing fatigue life, including tribological conditions, surface and sub-surface defects and environmental conditions (temperature, corrosion and humidity) [1]. In optimized working conditions, the main cause of damage in bearings is Rolling Contact Fatigue (RCF) [2] which involves two different phenomena: surface pitting and sub-surface spalling. The

main factor affecting sub-surface RCF damage is related to non-metallic inclusions, where the Hertzian contact shear stress is maximum [3]; in fact inclusions act as stress risers and then promoting crack initiation and propagation [4]. Steelmaking processes increased steel cleanliness [5, 6], but non-metallic and oxides inclusions cannot be removed completely even if they can be somehow controlled [7] and the effect of surface induced RCF failures can be reduced and eliminated with proper lubricant and elastodynamic lubrication.

The effect of inclusions on fatigue life, considering the effect of size, shape, location and composition is described in many experimental, analytical and numerical studies [8-10]. RCF is influenced by the dimension of the largest inclusion present in the material and it can be predicted by statistic methods [5]. In [9], experimental activities conducted on bearing ball steel are described. Chemical composition and size of inclusions are measured by means of X-ray spectroscopy and destructive testing; the specimens are then tested RCF conditions. It resulted that specimens with larger defects have a lower fatigue life and the chemical composition of the inclusions affects the damage as well. In particular, specimens containing Al_2O_3 or Al_2O_3 CaO inclusions showed a lower life if compared to specimens containing SiO_2 Al_2O_3 inclusions. To investigate the effect of inclusion size on fatigue life, in [8] controlled defects ere introduced by drilling small holes in the material. In [11], experimental and numerical activities explored the stress state in the material around the inclusion, where microstructural changes were observed, referred as “butterfly wings”, by means of FEM and Voronoi tessellation to develop a predictive model for stress distribution and crack initiation near the defect. Varying size, location and composition of the inclusion, it was found that RCF life is strongly affected by defect elasticity and position. The maximum Von Mises stress is found when high elastic modulus inclusions are present and located at a depth equal to 0,5 times the contact half width. Different inclusion sizes (ranging from 8 to 16 μm) were studied, but no strong influence on stress concentration was found. This result is partially in agreement to what found in [12] where a threshold dimension for the defect is found to affect fatigue life. This threshold is material related and it can be

found for high strength steels for bearing manufacturing, for example. In [11], the experimental evidence of the critical effect of larger inclusions on fatigue life is mainly due to the fact that statistically they can happen to be at the critical depth. In [1114] the effect of size, depth and elastic modulus of aluminum oxide inclusions in a steel matrix are explored on stress distribution and crack propagation with a FEM approach. According to [10], it was observed that high elastic modulus inclusions cause higher stress peaks, and a critical value of defect depth (0,75 times the contact half width) can be defined, where the Von Mises stress is maximum. A larger range of inclusion dimensions (5-20 μm), was investigated observing variation in stress areas, and not in maximum stress values. This paper was continued in [3] where a damage model is implemented to estimate damage and then butterfly wings formation and evolution, coupling the Eshelby equivalent inclusion model and the contact Hertzian solution. The damage model is applied to the case of a spherical inclusion and cylindrical contact. A wide numerical simulations are described but no experimental validation is presented. In [13], basing on the Eshelby method, the interaction between multiple inclusions (pairs, clusters and stringers) was investigated.

This paper presents an investigation on the effect of microinclusions on fatigue performance of a steel alloy (100Cr6) for rolling element manufacturing and on balls.

Fatigue damage and failure mechanisms are studied by means of experimental testing on test bench for both material and balls. An analytical model is implemented in a numerical dedicated solver, to relate life of rolling elements to the micro-inclusion parameters. In particular a dedicated 3D model implementing Eshelby model is developed to estimate the stress distribution around the microinclusion. The calculated stresses is used as input for a life model to estimate the life of the ball bearing. To consider the effect of microinclusion on ball life, bearing life model is modified considering ball spin and precession during shaft rotation. Then experimental and calculated cycle to failure are compared and failure microscopic analysis is be performed.

Final aim of the research is investigating whether a microinclusion threshold parameter could be defined.

2 Analytical background

Hertz theory estimates the superficial and sub-superficial stress distribution when two elastic bodies are compressed one against the other.

If non-metallic inclusions are located in the volume of one of the two compressed elastic bodies, and near the surface, they act like stress risers, leading to cracks and failure [14]. The increase of stress inside the inhomogeneity is quantifiable using the Eshelby microinclusion model [15]. This model is widely used in literature, maily to describe the stress and strain status around microinclusion. In [3], for example, the strain field due to Hertzian contact is coupled with the strain field due to the presence of microinclusion. In [13] the interaction of many microinclusions is investigated by superimposing single inclusion stresses and strain fields. In the present paper, the Eshelby model was implemented to simulate ,not a generic microinclusion, but a specific microinclusion which geometry, position and composition, was obtained according to experimental evidences. The calculated stress field was then used to calculate the equivalent Tresca stress field in the matrix around the microinclusion. This approach is confirmed considering that the maximum shear stress is considered to be the responsible stress component in failure [16, 17]. It can be observed that the Eshelby model considers static contact conditions while RCF of a dynamic fatigue phenomenon. Therefore experimental evidence [18] show that a static contact model can be assumed instead of a RCF model to capture the fatigue limit in case of hard and stiff inclusions for bearing steels under RCF.

The Eshelby model allows to compute the stress field around and inside an ellipsoidal inclusion. A region (inclusion) in an infinite homogeneous, isotropic and elastic medium (matrix) undergoes a change of shape and size. Eshelby found that, if the inclusion is ellipsoidal and the matrix, in which it is embedded, is subjected to a homogeneous load, the stress within the inclusion is uniform. This means that the elastic stress and strain does not change inside the inclusion.

Mura [19] defined an inclusion as a subdomain Ω in a domain T. The eigenstrain $\varepsilon^*_{ij}(x)$ is given in Ω and zero in T-Ω. This is the inclusion problem, as the elastic modulus is the same for both subdomain and domain. The displacement u_j, strain ε_{ij}, and stress σ_{ij} are expressed by [19]:

$$u_i(x) = -C_{kjmn} \int_{\Omega} \varepsilon^*(x') G_{ijk}(x - x') d\, x'$$

$$\varepsilon_{ij}(x) = -\frac{1}{2} \int_{\Omega} \left(C_{klmn} \varepsilon^*_{min}(x') G_{ijk}(x - x') + G_{ijk}(x - x') \right) \mathrm{d}x'$$

$$\sigma(x) = -C_{ijkl} \int_{\Omega} \left(C_{klmn} \varepsilon^*_{min}(x') G_{ijk}(x - x') \right) \mathrm{d}x' + \varepsilon^*_{kl}(x)$$

Where C_{ijkl} is the stiffness tensor, G_{ij} is the Green's function, x is the position vector and x' is the position of the point source. Since the strain and the stress fields inside the inclusion are uniform,

$$\varepsilon_{ij}(x) = S_{ijkl} \varepsilon^*_{kl} \quad \forall\, x \epsilon \Omega$$

where S_{kl} is the Eshelby tensor [19].

The strain field outside the inclusion is described by the equation:

$$\varepsilon_{ij}(x) = S_{ijkl} \varepsilon^*_{kl} \quad \forall\, x \epsilon (T - \Omega)$$

Then the stress can be calculated as follows:

$$\sigma_{ij}(x) = C_{ijkl} \varepsilon_{kl}(x)$$

3 Life-stress relation

In life models for components and for materials in elastic field, generally speaking, a relation is defined between stress (or load) and number of cycles. This happens, for example, in the well known Basquin relation for materials [20].

When comparing fatigue tests run on materials in different conditions, for example in axial or in rotating bending conditions, a correction factor needs to be applied to take into account for how much specimen volume undergoes maximum stress, let it all be the whole volume in axial tests and the volume close to surface in rotating bending tests. To do so, corrective factors are defined to extend fatigue limits experimentally obtained on laboratory conditions to different working conditions [21].

In case of components, corrective factors require a more complex definition to take into account of all the possible effects in working conditions. Let them be, as for example in bearings, lubrication, temperature, rotational speed, etc. [22]. In the case of bearings, these parameters are generally related to the damage which can occur in the weakest link in the chain, that is the races [23]. Damage, actually, occurs also in rolling bodies.

In case of rolling balls, estimation of life requires a more complex approach as, during rotation, the contact point is almost the same for races but changes for balls due to spin and precession. It is interesting to note that in most of papers investigating fatigue life of materials for bearing balls, tests are run on specimens like plates and rods [7, 24] thus well knowing the number of cycles to which material and microinclusion will be stressed. In case of rolling balls, a different approach is required. In order to determine, statistically, how often the inclusion is loaded, it is necessary to know the frequency with which the ball surface point, below which the inclusion is located, contacts the race (inner or outer). In [25] the following formulation is given:

$$BSF = \frac{D}{2d}\left(1 - \left(\frac{d}{D}cos\phi\right)^2\right)$$

where *BSF* is the ball spin frequency, *D* is the pitch diameter, *d* the ball diameter and ϕ the contact angle. The contact angle is defined as the angle between the line joining the points of contact of the ball and the raceways in the radial plane, along which the combined load is transmitted from the raceways, and the line perpendicular to bearing axis. It has to be noted that a fault in the ball strikes twice this frequency: once the inner race, once the outer race.

Ball spin frequency *BSF* estimates the total number of cycles which a ball rotates during a complete shaft cycle, assuming no slip. Actually, some slip is present and it is damaging [24], because the angle ϕ varies with the position of each rolling element in the bearing, due to the ratio of local radial to axial load changes. Then each rolling element has a different (in direction) effective rolling diameter and each ball tends to rotate at a different speed. The cage limits the deviation of the rolling elements from their mean position, thus causing some random slip. Rolling without slipping is impossible, it is

then necessary to consider also the transverse slip. In [26] a formula is proposed to estimate both slip due to spin and precession motions and then ball rotational velocity. Considering precessional and spin movements it is possible to estimate the frequency with which a point on a ball contacts the races during shaft revolution.

3.1 Life estimation in presence of microinclusions

If geometrical data and loading conditions of the tested bearings are applied, then it is possible to calculate how often the point below which a microinclusion lies, contacts the races. In particular it results that, for the investigated bearing balls (SKF BAHB-311396 B), *BSF* is 2,46 and the ratio between shaft revolution and tranversal slip is 40. Considering that inclusion is loaded twice during a complete rotation (once with inner race and once with outer race), the frequency with which there is a stress-riser inside the inhomogeneity is estimated every 20 shaft revolutions. The assumption that should be taken is that the transverse slip is not random but always in the same direction of rotation. It is furthermore assumed that the load is effective only if the contact happens when the microinclusion is exactly below the contact point.

Once the microinclusion loading frequency is calculated, it is possible to estimate ball life, in the case a microinclusion is present, according to Zaretsky model [27]. Let's consider the well known probabilistic bearing life formulation [22]:

$$L_{10} = LF_C \cdot \left(\frac{C_d}{P_{eq}}\right)^p$$

where p is the load-life exponent (3 for ball bearings and 10/3 for roller bearings), C_d is the dynamic load capacity for a rolling-element, P_{eq} is the equivalent load, defined as the combined and variable load around the circumference of a ball bearing, LF_C is the bearing life factor.

For angular contact ball bearings, the life factor LF_C is dependent from several factors including statistical parameters (obtained from Weibull distribution) and a parameter *LF,* describing the ball-race conformity effects at the inner and outer races [27].

It is possible to extend this formulation to balls and then to balls with microinclusions.

The dynamic load capacity, expressed in Newton, is [27]:

$$C_d = f_{cm}(i \cdot cos\phi)^{0,7}(tan\phi)Z^{\frac{2}{3}}d^{1,8}$$

where f_{cm} is material-geometry coefficient, i is the number of rows of rolling elements, Z is the number of rolling elements for each row i. The material-geometry coefficient f_{cm} depends on the bearing type, material, and the conformity between the rolling elements and the races. In particular the conformity factor varies between 0,505 and 0,570. In case the life factor is 1, then the conformity coefficient is 0,52.

For the presented case, the representative value of rolling-element bearing geometry and material coefficient (f_{cm}) was obtained from [27, 28] by linear interpolation of bearing envelope size value.

The parameter LF is normalized for ball bearings with inner-race and outer-race conformities of 52 percent.

$$LF = \left(\frac{S_{max,0.52}}{S_{max}}\right)^n$$

where S_{max} is the maximum contact stress (from Hertz theory) and n is the Hertz stress life exponent

$$n = c + \frac{2}{e}$$

where $c = 9$ for ball bearings.

The evaluation of LF is dependent on the geometry of the bearing, in this case, for angular thrust loaded ball bearing, the Ball-Inner race conformity effect (LFi) is calculated as:

$$LF_i = \left(\frac{\left(\frac{2}{d_e - d} + \frac{4}{d} - \frac{1}{0{,}52d}\right)^{\frac{2}{3}} \mu\nu_i}{\left(\frac{2}{d_e - d} + \frac{4}{d} - \frac{1}{f_g d}\right)^{\frac{2}{3}} \mu\nu_{0,52}}\right)^n$$

From Hertz contact theory, the dimensions for the pressure area is given in terms of transcendental functions μ and ν. The values of the product of the transcendental functions (μν) are tabulated in function of ball bearing envelope size (*S*) and they are different for the inner and outer races:

$$S = \frac{d \cdot cos\phi}{d_e}$$

The conformity of the races (*f*) is defined as the ratio between the race radius (R_r) and the ball diameter. The evaluation of *LF* is dependent on the geometry of the bearing, in this case, for angular thrust loaded ball bearing, they have been calculated the ball-inner race conformity effect (LF_i) and the Ball-Outer race conformity effect (LF_o). Transcendental function of Hertzian contact theory values have been obtained from [27] and they are reported in Table 1:

Table 1: transcendental function values of Hertzian Contact Theory

$\mu\nu_i$	1,654
$\mu\nu_o$	1,541
$\mu\nu_{0,52i}$	1,57
$\mu\nu_{0,52o}$	1,465

P_{eq} does not depend on the geometry of bearing, then a weighted average between the nominal load N_L applied to the bearing and of the load which would generate the value of Tresca stress of the inclusion. Given the Tresca stress inside the inclusion, it is possible to calculate the theorical load T_L that would produce the equivalent Tresca stress in the matrix corresponding to the stress given by the microinclusion, by means of simulations with the numerical solver.

The weighted average could be calculate knowing that inclusion is loaded once every 20 shaft-rotation:

$$P_{eq} = (19\ N_L + T_L)\frac{1}{20}$$

where N_L is the nominal load applied to the ball without microinclusion and T_L is the load that would produce a stress corresponding to the one generated by the microinclusion.

Finally, L_{10} is calculated assuming a shaft rotational speed of 690 rpm.

It has to be noted that, differently from [3], the nucleation and evolution of crack is neither described nor modelled. The failure is assumed to be statistically occurring when a threshold equivalent stress is reached in the ball, due to the presence of the microinclusion.

4 Materials and method

Aim of the research is to develop a life estimation model for bearing rolling elements including the effect of microinclusions. The model will consider composition, dimension, shape, distribution and position of microinclusions.

To this aim four topics will be investigated.

- The material properties. In particular rotating bending fatigue experimental campaigns will be analyzed on material specimens.
- Component behavior. In particular the results of fatigue testing of test bench of ball bearing will be presented.
- Analytical approach of microinclusion effect on stresses. In particular the Eshelby model will be applied to estimate the stress field surrounding a single microinclusion and the Moschovidis model [29] to take into account of the effect on stress of the interaction of microinclusions. The models will be applied to the failed specimens of both experimental campaigns, considering dimension, shape, position and composition of each single microinclusion.
- Damage models. Once the estimation of the effect of microinclusions on stresses is estimated, a fatigue life model will be applied to all fatigue data to evaluate both if the microinclusion “notch” effect model is reliable for these applications and if the fatigue life model is

reliable. In particular, if in the case of the materials the number of cycles to which the specimens underwent is known, in the case of rolling element a statistical approach is necessary due to the fact that during bearing rotation, the microinclusion is not always subjected to maximum stress due to ball slip and precession movements.

The research activity is composed by an analytical part, supported by a numerical code, and an experimental part, which includes rotating bending fatigue tests performed on specimens and ball bearings tests executed on RCF benches. When the specimen or a ball fails, an analysis of the fracture was made, evaluating the inclusion presence and characterization. The experimental tests provided real data about the inclusions; thanks to this data the stress distribution around the inclusion was calculated.

4.1 4 points rotating bending fatigue testing on specimens

For the 4 points rotating bending fatigue test the steel wire was cut in 150 mm bars and then straightened to nullify the curvature of the coil. Then, the bars were quenched (12 minutes @850°C). Specimens were obtained, according to the ISO 1143 Standard. Material is 100Cr6 (Young Modulus 210 GPa, Poisson ratio 0.35, Elastic limit up to 2500 MPa). This material is defined in international Standards as UNI 3097 and DIN 17230 as 100Cr6, AISI/SAE as 52100, AFNOR 35-565 as 100C6. Many researchers are dedicated to this steel, both with experimental and numerical approaches. In [30] an experimental investigation reports the fatigue resistance (10^8 cycles) in rolling contact fatigue conditions in the range of 1800-2300 MPa for Hertzian pressure. In [7] the effect of the different composition of microinclusion referring to processing techniques and performances is investigated, aiming at relating steelmaking, inclusion microstructure and life. In [12, 31] an investigation of Very High Cycle fatigue behavior of bearing steels is reported, referring to international Standards. In this paper the high sensitivity of high resistance steels to microinclusions and defects is analyzed with an empirical approach of LEFM. In these papers the fatigue limit is found to be about 850 MPa. In [12]

the microinclusions are assumed as spherical and if their dimension is higher than 11 μm then an asymptotic behavior is described. For smaller inclusions the fatigue limit is strongly reduced and the dependence is only empirically described.

In the present paper a Staircase [32] fatigue campaign was run at 3500 rpm, life target $5 \cdot 10^6$cycles and stress increment in Staircase testing $\Delta\sigma$=25MPa. After-failure analyses consists in an optical inspection on the fracture surface and SEM analysis, to know the chemical composition and dimension of the inclusions.

4.2 Test rig fatigue testing on bearing balls

The fatigue test of the balls was designed in order to single out the failure only on the balls, without damaging the inner ring, the outer ring and the cage.

In order to ensure the reliability of different tests and so to have the same test conditions, a process protocol, established since many years, was adopted. In the protocol, failures due to excessive contact stresses, high temperatures and vibrations were avoided.

The tested bearing mounts only one row of 7 balls (6 regular and one including a microinclusion), instead of 14 balls, to increase the contact pressure between the rings and the tested balls. The load is axial (34400N). The grease is the Shell Gadus S3 V220. The cleanliness during the assembly is mandatory, since any contamination of the lubricant can lead to a reduction in the bearing fatigue life.

The ball material is the same 100Cr6 and ball diameter 11,112 mm.

During the firsts 10 minutes, the load is only the 30% of the nominal one to obtain a homogeneous distribution of the lubricant and the optimal centering of the shaft. After this time, the load is raised until the nominal one. Every 5 minutes the load is released for 25 seconds to allow the spinning of the balls.

Each 20 hours the rigs are stopped so as to change the rings, the lubricant, the cages.

At every stop of the bench, it must be disassembled and cleaned. The components are completely inspected. When one ball fails, the after-failure analyses consists in a stereomicroscope inspection on

each failed ball, to evaluate if the failure started from an inclusion; a SEM analysis to know the chemical composition and the dimension of the inclusion; the inclusion depth was evaluated thanks to a gauge meter. The experimental campaign is described in [33].

4.3 Stress calculation

Since the inclusion depth was known, it was possible to calculate the stress at the corresponding position, both for spheres and specimens. The Tresca equivalent stresses were evaluated. These stresses are calculated including the stress increment related to microinclusion. The nominal stresses, calculated by means of De Saint Venant Theory in the case of specimens, or by means of Hertz Theory in the case of balls, are then modified by the Eshleby solver.

4.4 Numerical solver

Eshelby model [15, 34, 35] was implemented in a 3D numerical solver in Matlab environment, to estimate the stress distribution around the microinclusion, taking into account of dimension, shape, position and composition of microinclusions.

The model inputs are material and microinclusion mechanical properties (from SEM analysis), microinclusion geometry and distance from matrix free surface (from SEM analysis) and loading history. The code reads the input stress tensor at the correct depth and, with all the inclusion data, it calculates the incremented stress tensor and the Tresca and von Mises equivalent stresses due to microinclusion. It also plots in a 3D graph the stress state inside and outside the inclusion.

5 Results and discussion

5.1 Numerical solver

In Figure 1 the stress distribution according to Hertz theory, for applied load ball by means of test rig is plot. The tensor at the depth inclusion is the input of the code for following simulations. The results of the equivalent Tresca stresses obtained for the experimentally found microinclusions are reported in columns 8 of Table 2 and Table 3 for specimens and balls respectively. These values are in agreement with the ones simulated in [3].

In particular it can be observed the influence of main factors affecting the stress increment (according to De Saint Venant for specimens, and to Hertz for balls) due to the presence of microinclusions: microinclusion dimension, shape and depth. The inclusion size affects the stress field around the inclusion: increasing the inclusion dimension, the area, subjected to a stress perturbation, increases. On the other hand, the Tresca stress peak value does not change significantly. These results agree to [14] and [11]. Obviously, a larger inclusion can be located at the critical depth with a higher probability respect to a smaller one. For what concerns shape, varying the two semi axes of the inclusion perpendicular to the force direction (force directed along z axis), until one order of magnitude between the two semi axes, it results that the shape plays an important role on the stress increment at the inclusion boundary, if the semi axes ratio increases, the stress peak increases in a not negligible way.

Experimental evidence shows that inclusions can appear in pairs, clusters and stringers. In order to be aligned with experimental cases and to the ASTM E45 Standard [31], few cases have been considered for the numerical analysis. The Standard provides a solution for the stringer case, that is considered with a minimum of three particles. In this case, the stringer can be considered as a stand-alone inclusion with an elongated semi axis that covers the distance from the first to the last inclusion of the stringer. As suggested by the E45 [31], the particles have to be placed at a certain distance limit from the centerline of the stringer itself, and the distance between them has to be less than a certain

threshold. Considering a stringer as a standalone inclusion with elongated semi axis, it is similar to what has been found about shape effect.

An affecting factor, for the stress peak at the inclusion boundary, is the depth at which the inclusion is located. From the Hertz theory, it is known that the maximum equivalent stress is located at a certain depth below the surface. This depth can be identified, with a good approximation, as 75% of the contact half width. As proposed in [14], if the inclusion is far from the surface it will be not the main source of the spalling. According to the present research, in the worst case, the stress increase is approximately +50%. The depth threshold below which the stress remains below the maximum stress calculated by Hertz is approximately 188% the contact half width. This result is in good agreement with other numerical researches [3, 11, 14] and experimental investigations [30].

Most inclusions in bearing steels, are non metallic (NMI), and typically they are stiffer than the matrix. In fact, referring to experimental cases, few of the most common ones are Alumina (Al_2O_3), Titanium nitrides (TiN) and Titanium carbides (TiC) and each of them has an elastic modulus that is approximately 1.8 times or higher than the elastic modulus of the pure steel. Also other types of inclusions can be found, typically they are not detrimental as the ones presented above since they are not as stiff as those. In the cases presented here, the peak increment remains almost the same (between +36% and +39%), but this effect is due to the very similar Young modulus. Major changes on the elastic modulus will lead to larger increments, since they are related to the difference between the elastic modulus of microinclusion and matrix: if this difference increases, the peak increases. This analytical and numerical result is in agreement with what found empirically in [8].

Another parameter is the Poisson ratio of matrix and microinclusion. Similarly to what seen for the Young modulus, when the difference increases, also the peak stress increases.

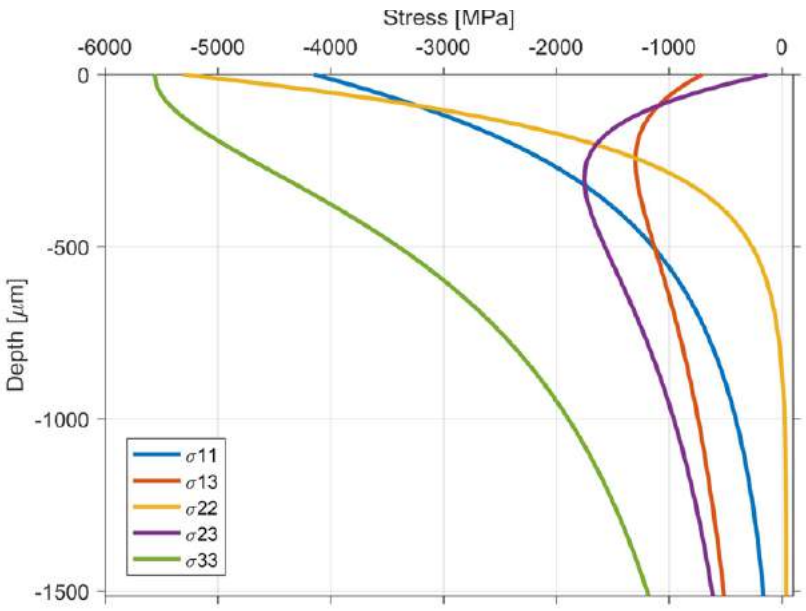

Figure 1: subsurface stress distribution according to Hertz theory, for applied load ball by means of test rig.

Numerical stress simulation shows a stress gradient in the matrix volume surrounding the microinclusion (see Figure 2 as an example), and an equivalent stress intensity factor, calculated as the ratio between Tresca equivalent stress in presence and in absence of the microinclusion, ranging between 1,21 and 1,36 for specimens and 1,20 and 1,57 for balls. In these conditions, it has to be observed that the stress intensity factor is calculated taking into account of the materials properties as the Tresca ideal stress is calculated with Eshelby model which takes into account of materials Young Modulus.

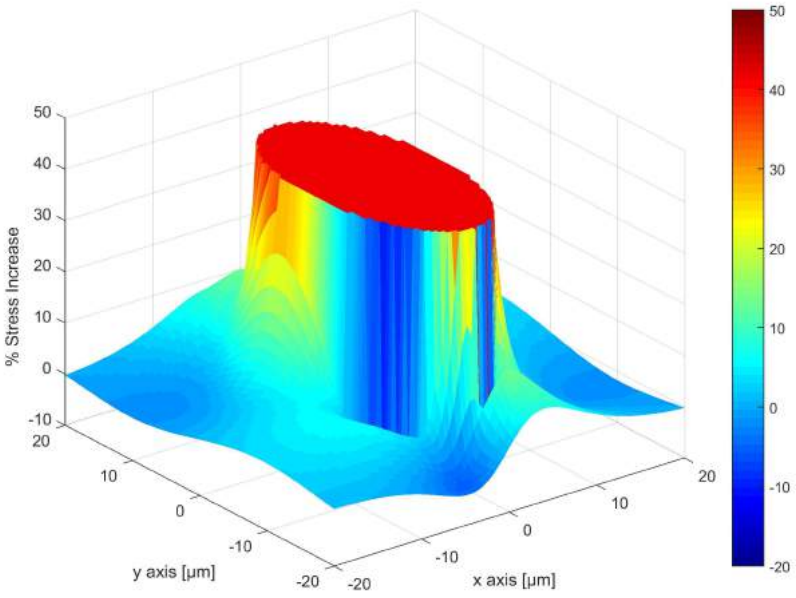

Figure 2. Simulation of stress distribution around microinclusion in balls. Case 3.

5.2 4 points rotating bending fatigue testing on specimens

In Table 2 the results of fatigue testing and calculation on specimens are reported. In particular in the same Table 2 the microinclusion composition and dimension along the three axes of global reference system, are reported, the depth with respect to ball surface at which microinclusion is positioned, the maximum equivalent Tresca stress σ_{nT} in the same position, assuming no microinclusion is present and maximum equivalent Tresca stress calculated by means of Eshelby model and numerical simulation, corresponding to the presence of the microinclusion σ_{iT}, the percent difference between the two maximum equivalent Tresca stress values σ_{inc} and the actual life of specimens with microinclusions. For what concerns microinclusion composition, when different compositions were found, the stiffer one Young modulus was assumed in calculations.

Seven failure cases were analyzed. The inclusion from which the fracture started, was composed by Al_2O_3 plus others oxides in five of the cases. Only in one specimen no Aluminum was found. The remaining specimen had an inclusion but probably it broke off when the rupture happened, so it was not possible to identify the inclusion composition.

It has to be noticed that when Al_2O3 was present, the Young modulus and the Poisson ratio were the ones of the Al_2O_3 itself, since they are the most critical in this case and it is very difficult to determine the factors taking into account every element. The inclusions were all similar also in terms of dimensions and depth, and basically they can be approximated as circular.No more than one inclusion was present in the fractured area.

When, as in case 3, the microinclusion is not present but it is possible to recognize the crater where it was positioned (Figure 3), then the measures of the crater were assumed as microinclusion dimensions and the traces of the element found in the craters helped to define the microinclusion composition.

Table 2: specimens fatigue results and calculation

Case	Microinclusion composition	Inclusion dimension			inclusion depth	σ_{nT} [MPa]	σ_{iT} [MPa]	σ_{inc} [%]	Cycles to failure
		x	y	z					
1	Al2O3	17,5	17,5	17,5	-245	501	683	36	2800000
2	Al2O3	13,5	13,5	13,5	-85	577	787	36	1360000
3	Al2O3	12,5	12,5	12,5	-80	555	756	36	2740000
4	S, Ca and Mn	12,5	12,5	12,5	-142	539	652	21	10100000
5	Al2O3	13,0	13,0	13,0	-34	591	805	36	770000
6	Al2O3	12,0	12,0	12,0	-74	580	791	36	620000
7	Al2O3	11,5	11,5	11,5	-138	563	767	36	60000

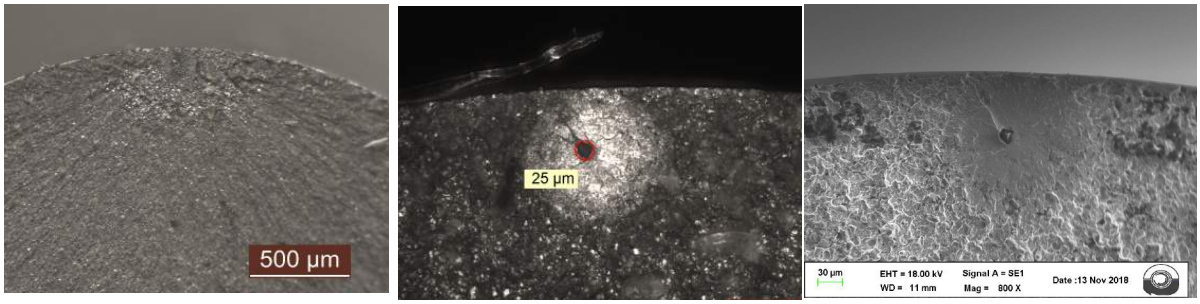

Figure 3: specimen 3 microinclusion crater.

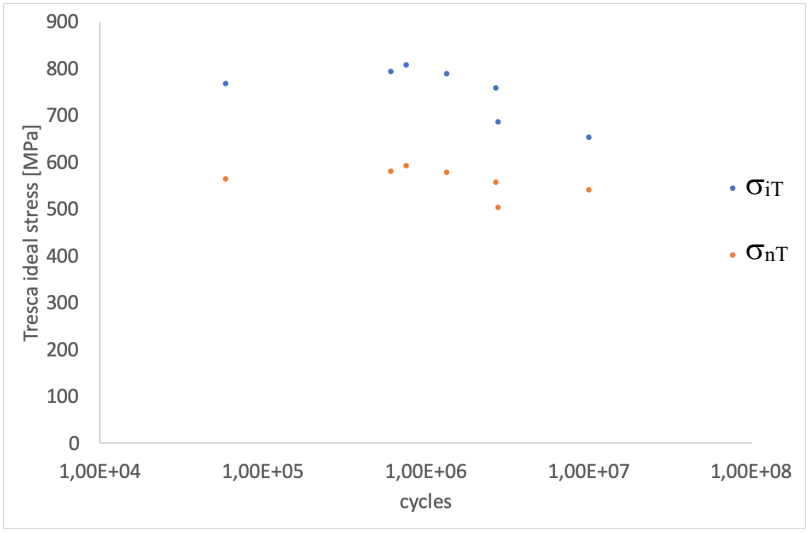

Figure 4: SN diagram for specimens

Figure 4 reports the SN diagram for specimens with microinclusions. In the vertical axis both the nominal Tresca stress (σ_{nT}) and the Tresca ideal stress calculated by means of Eshelby model and numerical simulator referring to true microinclusion data (σ_{iT}) are reported.

From numerical simulations, it results that the stress intensity effect due to microinclusions causes a stress increment of 1,21-1,36 times the nominal stress in the experimentally investigated cases. In these conditions, the stress does not reach the plastic range and, in the matrix, crack nucleation can be

attributed to fatigue phenomena, worsened by notch effects. SEM observations confirm this hypothesis (Figure 6 (a)).

5.3 Test rig fatigue testing on bearing balls

Seven broken balls coming from test rigs were analyzed. In five cases more than one inclusion was present in the fractured area: for this reason the considered one was the one with the major increase of stress, since it was the worse from the fatigue life point of view. Probably, also in the other two cases the balls had few inclusions, but it could happen that they remained under the material that was peeling. Regarding the chemical composition, if the presence of some elements was negligible (evaluating the spectrum) these elements were neglected when considering the composition. Otherwise, if the presence of some elements was not negligible, a weighted average of them was performed to obtain the Young modulus and the Poisson ratio. It happened that for some inclusions, the dimensions were not clear, as the chemical composition and so the Young and Poisson parameters.
In Figure 5 and in Table 3 the results of balls are reported. In Figure 5 it can be observed that numerical simulation results to be conservative for all failure cases but for case 4 and case 6. These two microinclusions are closer to the surface than the other and are bigger than the others. In particular their dimension lies in the dimensional range that in [36] is stated to be strongly affecting fatigue life. It apparently can be observed, according to these two data, that the Eshelby model coupled with statistical “stroke frequency” model better behaves for “small” microinclusions than for big ones, but more data are required. The L_{10} estimation without microinclusion (red vertical line) actually misses most of the failure which take place due to microinclusions.

Table 3: balls fatigue results and calculation

Case	Microinclusion composition	Inclusion dimension			inclusion depth	σ_{nT} [MPa]	σ_{iT} [MPa]	σ_{inc} [%]	Cycles to failure	L_{10} with microinclusions
		x	y	z						
1	TiC	1,7	4,3	1,7	-453	2319	3650	43	460000	940194
2	Al2O3	1,7	2,7	1,7	-562	2319	3189	37	1400000	979110
3	Al2O3	7,0	4,9	7,0	-600	2210	3146	42	1940000	976626
4	Al2O3	12,5	12,5	12,5	-284	2748	3743	36	870000	824274
5	TiC, SiO2	4,5	4,5	4,5	-436	2609	3168	21	1450000	1034586
6	Al2O3	12,3	10,0	10,0	-326	2759	3706	34	460000	873954
7	S, Mn, Ca	3,5	2,0	2,0	-450	2636	3173	20	3750000	1037484

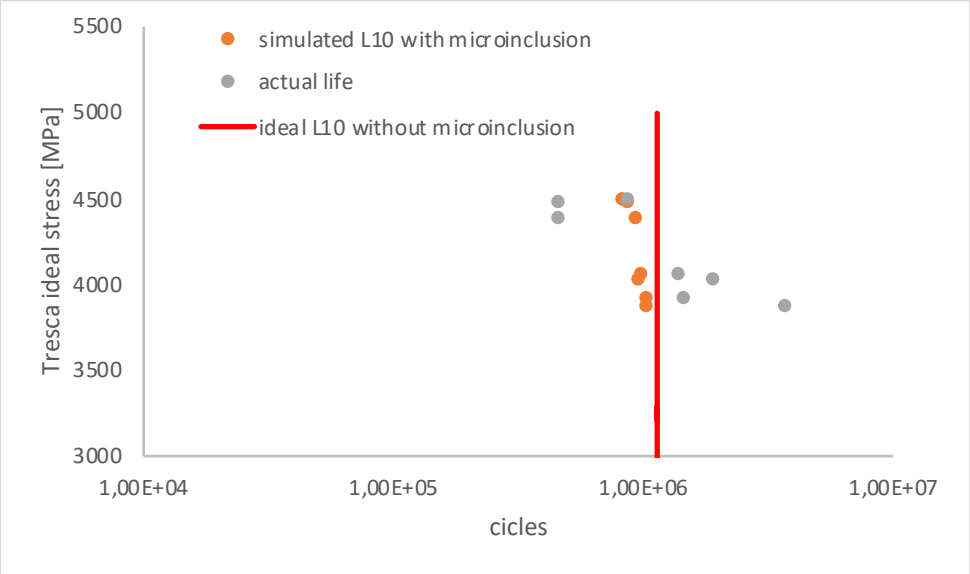

Figure 5: SN diagram for balls with microinclusions

From numerical simulations, it results that the stress intensity effect due to microinclusions causes a stress increment of 1.5 times the nominal stress in the experimentally investigated cases. In these

conditions, the stress reaches the plastic range and, in the matrix, crack can nucleate. From failure surface observations it resulted that the inclusion is not affected by failure process and the plastic phenomena affected the interface between matrix and inclusion (Figure 6 (b)). The consequent stress release can have restored nominal stresses in the matrix and then crack can have propagated in the matrix, slowly, until failure.

A further confirmation on effectiveness of the implemented approach can come if considering experiments run on balls which fits with the experimental curves reported in [30].

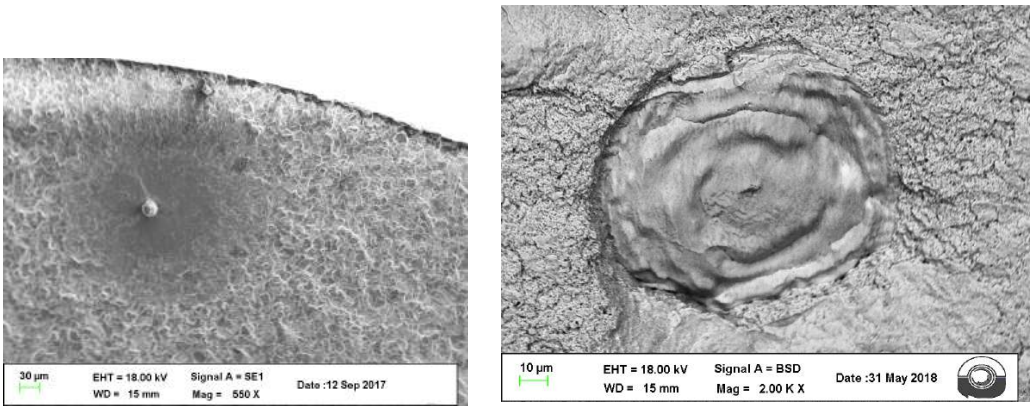

(a) *(b)*

Figure 6: failure surface around microinclusion for specimen (a) and balls (b)

Conclusions

The main target of the activity was to evaluate the influence of microinclusions on the fatigue life of rolling bodies. For this reason, the effect on the stress field of balls and specimens made of 100Cr6 was studied.

The spheres were tested thanks to a dedicated test rig, while a rotating bending fatigue machine was used for specimens. The fracture analyses were assessed thanks to a gaugemeter, an optical microscope and a Scanning Electron Microscope. A numerical solver that implements

the Eshelby solution for the inclusion problem was developed to analyze the cases above. Some simulations were made to understand the functionalities of the code and the effect of the different parameters: dimension, shape, depth, chemical composition and configuration were evaluated. Moreover, the code was useful to simulate the stress state of the experimental cases. Seven specimens and seven balls were considered, for each case all the inclusion properties were found and the stress state around microinclusion was evaluated.

A bearing life model including the effect of microinclusion was proposed. In particular bot a statistical approach and a deterministic description of spin and precession ball movement were implemented to estimate the frequency to which a microinclusion is subjected to maximum load.

The survey pointed out that inclusions that are shallower than a certain value are not critical for failures, according to [12, 31]. The difference between the Young modulus of the inclusion and the one of the matrix, as well as the Poisson ratio, is very important for the distribution of stress variation. Another key factor is the shape, if the inclusion can be approximated as an elongated ellipse, the stress peak increment is greater. There was a wide range of inclusion types found in balls, with also different shapes and dimensions, while in specimens they had similar properties.

Bearing life model, describing microinclusions effect, predicts ball's life better than L_{10} formula. Further discussion and further development of this approach can follow, considering that the elastic modulus of the matrix change during damaging processes, according to [3,24, 37, 38] and thus the estimation of Tresca stress by means of Eshelby model should take into account of this evolving phenomenon or, according to [3], couple the stress fields due to microinclusion and to Hertzian contact. Also the interaction between microinclusions can be modelled in a more detailed way, above all in the case they have different compositions.

6 References

1. Halme, J., Andersson, P.: Rolling contact fatigue and wear fundamentals for rolling bearing diagnostics-state of the art. Proceedings of the Institution of Mechanical Engineers, Part J: Journal of Engineering Tribology 224 (4), 377-393 (2010).
2. Arakere, NK.: Gigacycle rolling contact fatigue of bearing steels: A review. International Journal of Fatigue 93, 238-249 (2016).
3. Beyer T., Sadeghi F., Chaise T., Leroux J., Nelias D. 2019. A coupled damage model and a semianalytical contact solver to simulate butterfly wing formation around nonmetallic inclusions. International Journal of Fatigue, 127, 445-460.
4. Tsunekage, N., Hashimoto, K., Fujimatsu, T., Hiraoka, KS., Beswick, J., Dean, W.: Initiation behavior of crack originated from non-metallic inclusion in rolling contact fatigue. Journal of ASTM International 7(2), 1-9 (2010).
5. Unigame, Y., Hiraoka, K., Takasu, I., Kato, Y.: Evaluation procedures of nonmetallic inclusions in steel for highly reliable bearings. Bearing Steel Technology-Advances and State of the Art in Bearing Steel Quality Assurance: 7th Vol. ASTM International (2007).
6. Ebert, FJ.: Fundamentals of design and technology of rolling element bearings. Chinese Journal of Aeronautics 23 (1), 123-136 (2010).
7. Fu H, Rydel JJ., Gola AM., Yu F., Geng K., Lau C., Luo H., Rivera Diaz del Castillo PEJ. The relationship between 100Cr6 steelmaking, inclusion microstructure and rolling contact fatigue performance. International Journal of Fatigue, https://doi.org/10.1016/J.ijfatigue.2018.11.011
8. Makino, T., Makino, T., Neishi, Y., Shiozawa, D., Kikuchi S., Okada, S., Kajiwara, K., Nakai, Y.: Effect of defect shape on rolling contact fatigue crack initiation and propagation in high strength steel. International Journal of Fatigue 92, 507-516 (2016).
9. Hashimoto, K., Fujimatsu, T., Tsunekage, N., Hiraoka, K., Kida, K., Costa Santos, E.: Study of rolling contact fatigue of bearing steels in relation to various oxide inclusions. Materials & Design 32 (3), 1605-1611 (2011).

10. Murakami, Y., Naoko NY.: Influence of hydrogen trapped by inclusions on fatigue strength of bearing steel. Bearing Steel Technology. ASTM International, 2002.
11. Moghaddam, MS., Sadeghi, F., Paulson, K., Weinzapfel, N., Correns, M., Bakolas, V., Dinkel M.: Effect of non-metallic inclusions on butterfly wing initiation, crack formation, and spall geometry in bearing steels. International Journal of Fatigue 80, 203-215 (2015).
12. Gabelli A., Lai J., Lund T., Ryden K., Strandell I., Morales-Espejel GE., 2012. The fatigue limit of bearing steels – Part II: Characterization for life rating standards. International Journal of Fatigue, 38, 169-180.
13. Courbon, J., Lormand, G., Dudragne, G., Daguier, P., Vincent A.: Influence of inclusion pairs, clusters and stringers on the lower bound of the endurance limit of bearing steels. Tribology international 36 (12), 921-928 (2003).
14. Guan, J., Wang, L., Zhang, C., Ma, X.: Effects of non-metallic inclusions on the crack propagation in bearing steel. Tribology International. 106, 123-131. (2017).
15. Eshelby, JD.: The determination of the elastic field of an ellipsoidal inclusion, and related problems. Proc. R. Soc. Lond. A 241, 376-396 (1957).
16. Becker PC., Microstructural changes around non-metallic inclusions caused by rolling contact fatigue of ball bearing steels. Met Technol 1981. 8(1), 234-43
17. Grabulov A., Petrov R., Zandbergen HW. EBSD investigation of the crack initiationand TEM/FIB analyses of the microstructural changes around the cracks formed under rolling contact fatigue (RCF). International Journal of Fatigue 2010. 32(3), 576-83.
18. Allison B., Pandkar A., Critical factors for determining a first estimate of fatigue limit of bearing steels under rolling contact fatigue, International Journal of Fatigue, 2018, 117, 396-406.
19. Mura T. Micromechanics of defects in solid. Dordrecht, 1987
20. Basquin, OH., 1910. The exponential law of endurance tests. ASTM Proceedings, 10, 629-630
21. Fuchs HO.,, Stephens RI, Metal fatigue in Engineering, 2nd ed, Wiley, New York, 2000.
22. Rolling Bearings, 2018. SKF ed.

23. Sehgal R., Gandhi OP., Angra S., Reliability evaluation and selection of rolling element bearings. 2000. Reliability Engineering and System Safety, 68 (1), 39-52
24. Savolainen M., Lehtovaara A. 2018, An approach to investigating subsurface fatigue in a rolling/sliding contact, International Journal of fatigue, 2018, 117, 180-188.
25. Robert B. Randall, Jerome Antoni, Rolling element bearing diagnostics-a tutorial, 2010. Mechanical System and Signal processing. 25, 485-520
26. E.P. Kingsbury. Precessional slip in angular contact ball bearing. 1982. Wear, 77, 105-114.
27. Zaretsky., E.: Rollling bearing life predictions, theory and application. Recent Developments in Wear Prevention, Friction and Lubrication. 37, 2 (2010).
28. Zaretsky, EV., ed STLE Life Factors for Rolling Bearings. STLE SP-34, Society of Tribologist and Lubrication Engineers, Park Ridge, IL 1992.
29. Moschovidis ZA. Two ellipsoidal inhomogeneities and related problems treated by the equivalent inclusion method, Ph.D. Thesis, Northwestern University, Evanston 1975.
30. Oezel M., Janitzky T., Beiss P., Broeckmann C., 2019, Influence of steel cleanliness and heat treatment conditions on rolling contact fatigue of 100Cr6. Werar, 430-431, 272-279.
31. ASTM Int. Standard Methods for Determining the Inclusion Content of Steel, E45.
32. ISO 3964 Mechanical testing for metallic materials - Fatigue testing at room temperature. (in Italian) 1985.
33. Ossola,E., Pagliassotto S., Rizzo S., Sesana R. Microinclusion and Fatigue Performance of Bearing Rolling Elements, In: Structural Integrity - Mechanical Fatigue of Metals Experimental and Simulation Perspectives, Correia J.A.F.O., De Jesus A.M.P., Fernandes A.A., Calçada R., Springer International Publishing (Svizzera), Vol. 7, 321-326.
34. Guido, FL.: Develpopment of a methodology for geologic-geomechanic modelling and for monitoring of reservoirs dedicated to natural gas storage (in Italian). Ph.D.Thesis. University of Bologna, 2003.

35. Meng, C., Heltsley, W., Pollard, DD.: Evaluation of the Eshelby solution for the ellipsoidal inclusion and heterogeneity. Computers & Geosciences 40, 40–48 (2012).
36. Lai J., Lund T., Ryden K., Gabelli A., Strandell I., 2012. The fatigue limit of bearing steels – Part II: A pragmatic approach to predict very high cycle fatigue strength. International Journal of Fatigue, 37, 155-168.
37. Moghaddam S N., M., Sadeghi F., Paulson K., Weinzapfel N., Correns., Dinkel M. 2016., A 3D numerical and experimental investigation of microstructural alterations around non metallic inclusions in bearing steels. International Journal of Fatigue, 88, 29-41.
38. Kang JH., Rivera Diaz del Castillo EJ., 2014 Fatigue in martensitic 100Cr6: relationship between rolling contact fatigue microstructural transitions and repetitive push testing. 2014. Materials Science and Engineering, 614, 214-222.